STOML2 interacts with PHB to activate the MEK/ERK signaling pathway and mediates autophagy-related proteins in the progression of hepatocellular carcinoma

HAOYANG HU[1], HAOZHE ZHANG[2], SHUAI HAN[1], JIANLI CHEN[1] and YING XIE[3]

[1]Second Department of Hepatobiliary and Pancreatic Surgery, North China University of Science and Technology Affiliated Hospital, Tangshan, Hebei 063000, P.R. China; [2]Department of Urology, North China University of Science and Technology Affiliated Hospital, Tangshan, Hebei 063000, P.R. China; [3]Laboratory Animal Center, Hebei Medical University, Shijiazhuang, Hebei 050017, P.R. China

Received June 3, 2025; Accepted November 3, 2025

DOI: 10.3892/ijmm.2025.5709

Abstract. Hepatocellular carcinoma (HCC) treatment remains challenging due to the prevalence of metastasis and chemotherapy resistance. Mitochondrial stomatin-like protein 2 (STOML2), which is upregulated in various solid tumors, is associated with a poor prognosis; however, its biological function and molecular mechanism in HCC remain unclear. The present study aimed to elucidate the oncogenic mechanism of STOML2 in HCC and to explore its potential as a therapeutic target. Firstly, STOML2 expression in HCC and matched normal liver tissues was analyzed. In addition, STOML2-knockdown (HCCLM3-short hairpin RNA-STOML2) and -overexpression (Huh7-STOML2) cell models were established. Wound healing, Cell Counting Kit-8 and Transwell assays, and flow cytometry were performed to assess cell proliferation, invasion, migration and apoptosis *in vitro*. Furthermore, the biological function of STOML2 was confirmed *in vivo*. Co-immunoprecipitation (co-IP) and immunofluorescence staining were conducted to validate the interaction of STOML2 with prohibitin (PHB) following the prediction of binding partners. Downstream pathways regulated by STOML2 were identified using western blotting and were further investigated using the RAF1 inhibitor sorafenib. The present study revealed that STOML2 expression was significantly upregulated in HCC tissues and metastatic lesions, and was associated with poor patient prognosis. The *in vitro* experiments showed that STOML2 overexpression promoted proliferation, invasion, migration and autophagy, while inhibiting apoptosis in Huh7 cells. Conversely, STOML2 knockdown reversed these phenotypic changes. Furthermore, co-IP confirmed the direct interaction between STOML2 and PHB, which activated the RAF/MEK/ERK signaling pathway. The *in vivo* experiments further confirmed that STOML2 overexpression significantly accelerated tumor growth, whereas STOML2 or PHB knockdown inhibited tumor progression. In addition, sorafenib treatment suppressed STOML2-mediated cell migration and the expression of autophagy-related proteins by blocking the MAPK pathway. These findings elucidated the molecular mechanism by which STOML2 promotes the malignant progression of HCC and demonstrated that targeted inhibition of the PHB-MAPK pathway may reverse the pro-tumorigenic effects of STOML2. STOML2 may serve as both a prognostic biomarker and a therapeutic target in HCC. The current study provides a theoretical foundation for individualized treatment in patients with HCC and high STOML2 expression.

Correspondence to: Dr Jianli Chen, Second Department of Hepatobiliary and Pancreatic Surgery, North China University of Science and Technology Affiliated Hospital, 73 Jianshe South Road, Lubei, Tangshan, Hebei 063000, P.R. China
E-mail: huhaoyang225@126.com

Dr Ying Xie, Laboratory Animal Center, Hebei Medical University, 361 Zhongshan East Road, Shijiazhuang, Hebei 050017, P.R. China
E-mail: xieying@hebmu.edu.cn

Abbreviations: co-IP, co-immunoprecipitation; HCC, hepatocellular carcinoma; IF, immunofluorescence; PHB, prohibitin; STOML2, stomatin-like protein 2

Key words: HCC, STOML2, PHB, MAPK signaling pathway, proliferation, autophagy

Introduction

Primary liver cancer is the sixth most common type of cancer and the second leading cause of cancer-associated mortalities worldwide (1) with a 10-year survival rate of 8.2% (2). Although notable advances have been made in cancer research over recent decades, major challenges persist in the treatment of cancer. Malignant invasion, recurrent metastases and chemoresistance remain the primary contributors to disease relapse (3). Hepatocellular carcinoma (HCC) is typically diagnosed at an advanced stage, making curative surgical intervention difficult. Currently, the clinical efficacy of molecular targeted therapies and immunotherapies for HCC is limited by factors such as drug resistance and tumor recurrence (4). This limitation underscores the need to elucidate the molecular mechanisms driving HCC progression and

to identify novel therapeutic targets, thereby laying a strong scientific foundation for the development of more effective treatment strategies (5).

Stomatin-like protein 2 (STOML2, also known as SLP-2) is a unique member of the stomatin family, encoded by a gene located on chromosome 9p13 (6). A defining structural feature of STOML2 is the absence of the N-terminal hydrophobic domain found in other homologous proteins (7). STOML2 is predominantly localized to the inner mitochondrial membrane, where it faces the intermembrane space, and participates in the regulation of mitochondrial biogenesis and energy metabolism through interactions with inner membrane components (8,9). Notably, a previous study demonstrated that upregulation of STOML2 is closely associated with the development of various tumors (10,11), highlighting its potential functional importance.

Currently, a growing body of research has suggested that STOML2 exhibits dysregulated expression in various malignant tumors. STOML2 has been reported to be upregulated in ovarian cancer (10,12), gastric cancer (13), papillary thyroid carcinoma (14), colorectal cancer (15), gallbladder cancer (11), HCC (16), and squamous cell carcinoma of the head and neck (17). While STOML2 upregulation has been observed in HCC, its precise molecular mechanisms, particularly its role in metastasis, signaling pathways and interaction with prohibitin (PHB), remain largely uncharacterized. Malignancy is increasingly recognized as a progressive and chronic disease (18). For example, HCC is typically secondary to persistent liver injury, and its characteristic pathological changes include excessive release of various cytokines, such as IL-6 and TNF-α, and aberrant vascularization (19). These pathological features not only markedly increase the complexity of clinical treatment but also critically influence long-term prognosis. Therefore, elucidating the molecular mechanisms underlying tumor progression, identifying novel biomarkers for HCC and its prognosis, and establishing new therapeutic targets hold scientific and clinical importance. The present study aimed to investigate the pro-tumorigenic role of STOML2 in HCC. The study aimed to determine whether its effects are mediated through an interaction with PHB and the subsequent activation of the MAPK signaling pathway. Furthermore, the therapeutic potential of targeting this axis, in combination with sorafenib, was explored for STOML2-upregulated HCC.

Materials and methods

Clinical samples. The present study is a retrospective analysis that enrolled a cohort of 72 patients with histologically confirmed HCC who underwent surgical resection at the North China University of Science and Technology Affiliated Hospital (Tangshan, China). Patient recruitment and sample collection took place between January 2015 and December 2023. The cohort had a mean age of 65 years (median: 63.5 years; range: 42-82 years) with a male-to-female ratio of 2.5:1. Fresh tumor tissues and matched adjacent non-tumor liver tissues (obtained >2 cm from the tumor margin) were collected, fixed in 4% neutral-buffered formalin at room temperature for 24 h and processed into paraffin-embedded blocks for subsequent analysis. The inclusion criteria were as follows: i) Pathologically confirmed primary HCC; ii) no prior chemotherapy or radiotherapy; iii) availability of complete clinicopathological data. Key exclusion criteria included: i) A history of other malignancies; ii) any anticancer treatment before surgery; iii) inadequate tissue sample quality. The study protocol was approved by the Ethics Committee of the North China University of Science and Technology Affiliated Hospital (approval no. 20250403024), and written informed consent was obtained from all participants.

Cell culture. The liver cancer cell lines HCCLM3, HepG2, Hep3B, MHCC97L and Huh7, the non-tumorigenic human hepatocyte cell line THLE-2 and 293T cells were purchased from Xiamen Yimo Biotechnology Co., Ltd. The cells were cultured in Dulbecco's modified Eagle medium (DMEM; Gibco; Thermo Fisher Scientific) supplemented with 10% fetal bovine serum (FBS; Gibco; Thermo Fisher Scientific, Inc.), 100 U/ml penicillin and 0.1 mg/ml streptomycin at 37˚C in a humidified atmosphere containing 5% CO_2. All cell lines were authenticated using short tandem repeat profiling.

Establishment of overexpression and knockdown cell lines. STOML2 knockdown was achieved using a short hairpin RNA (shRNA; shSTOML2) cloned into the psi-LVRH1P-Puromycin lentiviral vector (MailGene Scientific). For overexpression, the STOML2-coding sequence was cloned into the pCDH-CMV-MCS-EF1-T2A-Puromycin vector (MailGene Scientific). PHB knockdown (shPHB) was similarly achieved using a shRNA cloned into the psi-LVRH1P-Puromycin vector (MailGene Scientific). The shRNA sequences (5'-3') were as follows: shSTOML2-1, GCTCAAACAACCATGAGATCA; shSTOML2-2, GGAAATTGTCATCAACGTGCC; shPHB, GAAATCACTGTGAAATTT. A non-targeting scrambled shRNA (Scr) was used as a negative control for knockdown experiments, with the following sequence: 5'-GCTTCGCGCCGTAGTCTTA-3'; this was cloned into the same psi-LVRH1P-Puromycin vector. For overexpression experiments, the 'Mock' condition refers to cells transduced with the empty pCDH-CMV-MCS-EF1-T2A-Puromycin vector. The Huh7-STOML2 cell line refers to Huh7 cells stably infected with the STOML2 overexpression plasmid.

Lentiviral particles were produced using a second-generation packaging system. Briefly, 293T cells were co-transfected with 2.0 μg target plasmid, 1.5 μg packaging plasmid psPAX2 (cat. no. V010353; NovoPro Bioscience Co., Ltd.) and 0.5 μg envelope plasmid pMD2.G (cat. no. V010404; NovoPro Bioscience Co., Ltd.) in a 4:3:1 ratio using Lipofectamine® 3000 (Invitrogen; Thermo Fisher Scientific, Inc.) for 48 h at 37˚C. Viral supernatants were collected 48 h post-transfection, filtered and used to transduce target cells (HCCLM3 and Huh7) in the presence of 8 μg/ml polybrene (Biosharp Life Sciences). The multiplicity of infection was optimized to 10 for each cell line. Transduction was carried out for 24 h, after which the virus-containing medium was replaced with fresh complete medium. A total of 48 h post-transduction, cells were selected with 1.5 μg/ml puromycin (cat. no. BL528A; Biosharp Life Sciences) (for 1 week to establish stable polyclonal populations). The puromycin concentration for maintenance was reduced to 0.75 μg/ml. Infection efficiency was confirmed using reverse transcription-quantitative polymerase chain reaction (RT-qPCR) and western blotting.

RNA extraction and RT-qPCR. Total RNA was extracted from HCC cells and frozen tissue samples (stored at -80˚C) using TRIzol® reagent (Invitrogen; Thermo Fisher Scientific, Inc.). cDNA was synthesized from 1 μg total RNA using the PrimeScript™ RT Kit (Takara Biotechnology Co., Ltd.) in accordance with the manufacturer's protocol. Briefly, the RT reaction was carried out at 37˚C for 15 min, followed by inactivation at 85˚C for 5 sec. qPCR was performed using the QuantStudio® 3 Real-Time PCR system (Applied Biosystems; Thermo Fisher Scientific, Inc.) with SYBR Green Premix Pro Taq HS qPCR Kit (Hunan Accurate Bio-Medical Technology Co., Ltd.). The qPCR thermocycling conditions were as follows: Initial denaturation at 95˚C for 30 sec; followed by 40 cycles of denaturation at 95˚C for 5 sec and annealing/extension at 60˚C for 30 sec. Gene expression was quantified using the $2^{-\Delta DCq}$ method (20), with GAPDH as the endogenous control. All reactions were performed in triplicate. The primers used were as follows: STOML2, forward 5'-GCAGAAGGGAAG AAACAGGC-3' and reverse 5'-GAGAACGCGCTGACA TACTG-3'; PHB, forward 5'-AGAGAGAGCTGGTCTCTCC AGG-3' and reverse 5'-TCCACCGCTTCTGTGAACTC-3'; and GAPDH, forward 5'-CCAGCAAGAGCACAAGAGGA-3' and reverse 5'-GGGGAGATTCAGTGTGGTGG-3'.

Western blotting and co-immunoprecipitation (co-IP). Total proteins were extracted from frozen HCC tissues and cultured cells using RIPA lysis buffer (cat. no. WB3100; Suzhou NCM Biotech Co., Ltd.) supplemented with protease and phosphatase inhibitors. Protein concentrations were determined using the BCA Protein Assay Kit (cat. no. WB6501; Suzhou NCM Biotech Co., Ltd.). A total of 20 μg protein lysate/lane was separated by SDS-PAGE on 10% gels and transferred onto PVDF membranes (MilliporeSigma). The membranes were blocked with 1% bovine serum albumin (BSA; cat. no. A8010; Beijing Solarbio Science & Technology Co., Ltd.) for 1 h at room temperature. Subsequently, the membranes were incubated overnight at 4˚C with primary antibodies (1:500) specific to the target proteins STOML2 (cat. no. 10348-1-AP; Proteintech Group, Inc.), PHB (cat. no. GB113098-100; Wuhan Servicebio Technology Co., Ltd.), p62 (cat. no. 18420-1-AP; Proteintech Group, Inc.), Beclin1 (cat. no. 11306-1-AP; Proteintech Group, Inc.), RAF1 (cat. no. 26863-1-AP; Proteintech Group, Inc.), phosphorylated (p)-RAF1 (cat. no. 9427; Cell Signaling Technology, Inc.), MEK1/2 (cat. no. 11049-1-AP; Proteintech Group, Inc.), p-MEK1/2 (cat. no. 9154; Cell Signaling Technology, Inc.), ERK1/2 (cat. no. 11257-1-AP; Proteintech Group, Inc.), p-ERK1/2 (cat. no. 80031-1-RR; Proteintech Group, Inc.) and GAPDH (cat. no. 60004-1-Ig; Proteintech Group, Inc.). After washing with TBS-0.1% Tween-20 to remove unbound primary antibodies, the membranes were incubated with HRP-conjugated secondary antibodies (cat. no. ZB-2301; Beijing Solarbio Science & Technology Co., Ltd.) for 1 h at room temperature. After incubation, the protein bands were visualized using an enhanced chemiluminescent kit (cat. no. WP20005; Thermo Fisher Scientific, Inc.) according to the manufacturer's instructions. Images of the blots were captured and the band intensity was semi-quantified using Image Lab software (version 6.1; Bio-Rad Laboratories, Inc.).

For the co-IP assay, STOML2 was expressed as a Flag-tagged fusion protein and PHB was expressed as a Myc-tagged fusion protein. The coding sequences were cloned into the pCDH-CMV-Flag (cat. no. HSE067321; MailGene Scientific) and pCDH-CMV-Myc (cat. no. HSH067460; MailGene Scientific) vectors, respectively. For transfection, 293T cells were seeded at a density of $5x10^5$ cells/well in a 6-well plate and grown to 70-80% confluence. They were co-transfected simultaneously with a total of 2 μg plasmid DNA (Flag-STOML2 and Myc-PHB constructs at a 1:1 ratio) using Lipofectamine 3000 according to the manufacturer's instructions. The transfection complex mixture was incubated with the cells for 24 h at 37˚C. The cells were harvested 48 h post-transfection and lysed with IP Lysis Buffer (cat. no. 87787; Thermo Fisher Scientific, Inc.) on ice for 30 min. Cell debris was removed using centrifugation at 12,000 x g for 15 min at 4˚C. The supernatant was then collected and the protein concentration was determined using the BCA Protein Assay Kit. A total of 400 μg protein lysate was used for each IP reaction. Lysates were pre-cleared by incubation with 20 μl Protein A/G agarose beads (cat. no. sc-2003; Santa Cruz Biotechnology, Inc.) for 1 h at 4˚C with gentle agitation. The pre-cleared supernatants were then incubated overnight at 4˚C with the appropriate antibodies: Anti-Flag antibody (1:500 dilution; cat. no. 66008-4-Ig; Proteintech Group, Inc.) for immunoprecipitating Flag-STOML2 or normal rabbit IgG (1:500 dilution; cat. no. 30000-0-AP; Proteintech Group, Inc.) was used as a negative control. Anti-Myc antibody (1:500 dilution; cat. no. 60003-2-Ig; Proteintech Group, Inc.) was used to for immunoprecipitating Myc-PHB or normal rabbit IgG was used as a negative control. The following day, 30 μl Protein A/G agarose beads were added to each sample, and each sample was incubated for an additional 4 h at 4˚C to capture the antibody-antigen complexes. The beads were then collected using centrifugation at 1,000 x g for 5 min at 4˚C and washed three times with the same IP Lysis Buffer. After the final wash, the bound proteins were eluted from the beads by boiling in 2X SDS-PAGE loading buffer at 95˚C for 10 min. The eluted proteins were then separated by SDS-PAGE and analyzed using western blotting as aforementioned.

Immunofluorescence (IF) staining. Each of the three HCC cell lines (HCCLM3, HepG2 and Huh7) were seeded on a coverslip placed in a 6-well plate at a density of $2x10^4$ cells/well. After overnight incubation at 37˚C, the cells were washed twice with PBS, fixed with 4% paraformaldehyde for 20 min and permeabilized with 1% Triton X-100 for 5 min at room temperature. The cells were blocked in 5% BSA for 1 h at room temperature and then incubated with the following primary antibodies at 4˚C overnight: STOML2 rabbit antibody (1:200 dilution; cat. no. 10348-1-AP; Proteintech Group, Inc.) and PHB mouse antibody (1:200 dilution; cat. no. 60092-1-Ig; Proteintech Group, Inc.). The next day, the cells were incubated with the corresponding secondary antibody [Goat Anti Rabbit IgG (H+L) conjugated to Alexa Fluor 488 (1:500;cat. no. A32731TR); Goat Anti-Mouse IgG (H+L) conjugated to Alexa Fluor 594 (1:500 dilution; cat. no. A32742); both Invitrogen; Thermo Fisher Scientific, Inc.] for 1 h at room temperature in the dark and then counterstained with 1 μg/ml DAPI for 10 min at room temperature. Finally, the stained cells were observed and images were captured under a fluorescence microscope (400857; Nikon Corporation). For each

experimental group, at least five random fields of view were captured and analyzed.

Cell proliferation assay. For the Cell Counting Kit-8 (CCK-8) assay, 3,000 cells were seeded in each well of 96-well plates, and were incubated for 24, 48, 72 and 96 h at 37˚C. Prior to each measurement, the culture medium was removed and replaced with fresh medium containing CCK-8 reagent (Beijing Solarbio Science & Technology Co., Ltd.). After 1 h of incubation in a cell culture incubator, absorbance at 450 nm was measured using a microplate reader (Tecan Group, Ltd.) at the indicated time points.

Wound healing assay. Cell migration was also assessed using a wound healing assay. HCC cells were seeded in 6-well plates and grown to 100% confluence. To eliminate the influence of cell proliferation, the cells were serum-starved by replacing the growth medium with serum-free medium for 12 h prior to wounding and throughout the duration of the assay. A linear wound was then created using a 200-μl pipette tip, the wound area was marked and the plates were incubated under standard culture conditions for 24 h. Subsequently, the cells were fixed with 4% paraformaldehyde for 15 min at room temperature, stained with 0.1% crystal violet for 20 min at room temperature and images were captured under an inverted light microscope (Nikon Corporation). The results were semi-quantified by measuring the wound width at 0 and 24 h using ImageJ software (version 1.53t; National Institutes of Health). The percentage of wound closure was calculated as follows: [(Wound width at 0 h-Wound width at 24 h)/Wound width at 0 h] x100.

Cell invasion assay. Cell invasion was quantified using the Matrigel-coated Transwell assay. Transwell inserts (pore size, 8 μm; Corning, Inc.) were pre-coated with 100 μl Matrigel matrix (1 mg/ml; cat. no. 356234; Corning, Inc.) and incubated at 37˚C for 6 h to form a gel. A total of $1x10^5$ cells in 500 μl serum-free DMEM were seeded into the upper chamber of coated inserts. The inserts were placed in 24-well plates containing 500 μl DMEM supplemented with 10% FBS in the lower chamber. After 24 h, the cells that had migrated to the lower chamber were fixed with 4% paraformaldehyde for 15 min at room temperature, stained with 0.1% crystal violet for 20 min at room temperature and images were captured under an inverted light microscope for quantification. All experiments were performed in triplicate.

Immunohistochemistry (IHC). Tissue sections fixed in 4% neutral-buffered formalin at room temperature for 24 h were embedded in paraffin (4 μm) and were sequentially deparaffinized in xylene and rehydrated in a graded ethanol series (50, 70, 85, 95 and 100%). For antigen retrieval, slides were heated in 10 mM sodium citrate buffer (pH 6.0) using a microwave at 100˚C for 20 min. After cooling, endogenous peroxidase activity was quenched by incubating the sections with 3% hydrogen peroxide for 15 min at room temperature. Subsequently, the sections were blocked with 5% normal goat serum (cat. no. C0625; Beyotime Biotechnology) for 1 h at room temperature. The sections were then incubated overnight at 4˚C with primary antibodies against STOML2 (1:300 dilution; cat. no. 10348-1-AP; Proteintech Group, Inc.) or Ki-67 (1:300 dilution; cat. no. 27309-1-AP; Proteintech Group, Inc.) diluted in blocking buffer. After washing, the sections were incubated for 1 h at room temperature with HRP-conjugated secondary antibodies. Bound antibodies were visualized using a DAB substrate kit (cat. no. k346889-2; Dako; Agilent Technologies, Inc.) according to the manufacturer's instructions. STOML2 expression was assessed via IHC staining by two independent pathologists who were blinded to all clinical data. Staining intensity was graded on a scale of 0 (negative) to 3 (strong). The percentage of positive tumor cells was scored as 0 (0%), 1 (1-25%), 2 (26-50%), 3 (51-75%) or 4 (76-100%). A final IHC score was derived by multiplying the intensity and proportion scores, yielding a value between 0 and 12. Any discrepant assessments were resolved through a joint re-evaluation to reach a consensus. Stained sections were observed and images were captured under a light microscope (Nikon Corporation).

Hematoxylin and eosin (H&E) staining. Formalin-fixed, paraffin-embedded tumor tissues were sectioned at a thickness of 4 μm. Sections were deparaffinized in xylene, rehydrated through a graded ethanol series and stained with hematoxylin at room temperature (cat. no. C0107-100; Beyotime Biotechnology) for 5 min. After washing, the sections were differentiated in 1% acid ethanol, blued in Scott's tap water (cat. no. S5134; Sigma-Aldrich; Merck KGaA) and counterstained with 1% eosin Y (cat. no. 318906; Sigma-Aldrich; Merck KGaA) solution for 2 min. Finally, the sections were dehydrated, cleared in xylene and mounted with a synthetic mounting medium for light microscopy (Eclipse E100; Nikon Corporation).

MAPK pathway inhibition using sorafenib. For MAPK pathway inhibition, Huh7 cells overexpressing STOML2 were pre-treated with sorafenib (20 μM; cat. no. HY10201; MedChemExpress) for 24 h at 37˚C prior to subsequent assays, including western blotting, flow cytometry and functional assays. An equal volume of DMSO (cat. no. HY-Y0320; MedChemExpress) was used as the vehicle control in all experiments. The final concentration of DMSO in the culture medium did not exceed 0.1%.

Flow cytometry. For cell cycle analysis, ~$1x10^6$ cells were washed with PBS and fixed in 70% ice-cold ethanol at -20˚C for ≥2 h. Fixed cells were then pelleted, washed with PBS and treated with 100 μg/ml RNase A at 37˚C for 30 min from the Cell Cycle Detection Kit (cat. no. C1052; Beyotime Biotechnology) to remove RNA. Cellular DNA was then stained with 50 μg/ml PI in the dark at room temperature for 30 min according to the manufacturer's instructions. The stained cells were incubated in the dark at room temperature for 30 min and analyzed using a flow cytometer (BD Accuri C6; BD Biosciences). The percentages of cells in the G_0/G_1, S and G_2/M phases of the cell cycle were determined from the DNA histograms using software FlowJo (version 10.8.1; BD Biosciences).

Cell apoptosis was assessed using an Annexin V-FITC/PI Apoptosis Detection Kit (cat. no. 556547; BD Biosciences). Cells were harvested, washed twice with cold PBS and resuspended in 1X Binding Buffer at a density of $1x10^6$ cells/ml.

Subsequently, a 100-μl aliquot of the cell suspension was incubated with 5 μl Annexin V-FITC and 5 μl PI for 15 min at room temperature in the dark. Following incubation, 400 μl 1X Binding Buffer was added to each tube, and the cells were analyzed by flow cytometry (BD Accuri C6; BD Biosciences) within 1 h. Data were analyzed using the software FlowJo (version 10.8.1; BD Biosciences).

Animal experiments. The animal experiments performed in the present study were approved by the Animal Ethics Committee of North China University of Science and Technology (Tangshan, China; approval no. 2025SY3011).A total of 35 BALB/c male nude mice (age, 4-5 weeks; weight, 18-22 g) were purchased from Beijing Vital River Laboratory Animal Technology Co., Ltd. Mice were housed under specific pathogen-free conditions at a controlled temperature of 24˚C and humidity of 50%, under a 12-h light/dark cycle. To establish a subcutaneous HCC model, mice were randomly divided into seven groups (n=5/group), as follows: Group 1, injected with HCCLM3-Scr cells; Group 2, injected with HCCLM3-shSTOML2-1 cells; Group 3, injected with HCCLM3-shSTOML2-2 cells; Group 4, injected with Huh7-mock cells; Group 5, injected with Huh7-STOML2 cells; Group 6, injected with Huh7-STOML2-Scr cells; Group 7, injected with Huh7-STOML2-shPHB cells. A total of $3x10^6$ cells suspended in 200 μl PBS were injected subcutaneously into the dorsal neck region of each mouse. The experiments conducted on these mice included: Monitoring of tumor growth kinetics, final tumor weight measurement upon resection and IHC. After 25 days, mice were euthanized by gradual displacement of chamber air with CO_2 at a flow rate of 35% of the chamber volume/min, after which death was confirmed by the absence of a heartbeat and fixed, dilated pupils. Tumor width (W) and length (L) were measured weekly using vernier calipers, and tumor volume (mm^3) was calculated as follows: (W2 x L)/2. The humane endpoint criteria for euthanasia were as follows: i) If a mouse lost 15-20% of its initial body weight, or exhibited noticeable emaciation and muscle atrophy; ii) if the mouse completely lost its appetite for 24 h, or was unable to eat or drink independently; iii) if signs of distress or discomfort were observed, such as excessive scratching of a tumor leading to skin bleeding; and iv) if the tumor became ulcerated and infected, grew rapidly or impaired the normal feeding and behavior of the animal. After any of the criteria was met, mice were euthanized and tumors were isolated. The largest tumor volume in nude mice was 0.843 cm^3 and the largest diameter was 0.85 cm. None of the pre-defined humane endpoints were reached prior to the scheduled endpoint of the study.

Bioinformatics analysis. The online tool Gene Expression Profiling Interactive Analysis (GEPIA) (http://gepia.cancer-pku.cn/) was employed to generate the Kaplan-Meier overall survival curve. For this analysis, The Cancer Genome Atlas (TCGA) Liver Hepatocellular Carcinoma (LIHC) cohort was used, which includes data from 371 patients with primary LIHC. Patients with STOML2 expression levels above the median were classified as the 'High-expression' group, whereas those with expression levels below the median constituted the 'Low-expression' group. The corresponding clinical information for the LIHC cohort was downloaded from TCGA (https://portal.gdc.cancer.gov/projects/TCGA-LIHC).

For independent validation of STOML2 expression, two Gene Expression Omnibus (GEO) datasets were analyzed: GSE40367 (21,22) and GSE14520 (23). The GSE40367 dataset (https://www.ncbi.nlm.nih.gov/geo/query/acc.cgi?acc=GSE40367) includes profiles from 6 healthy control patient tissues, 10 primary HCC tumors and 18 metastatic HCC lesions. The GSE14520 dataset (https://www.ncbi.nlm.nih.gov/geo/query/acc.cgi?acc=GSE14520) comprises 22 paired normal liver tissues and 22 HCC tissues. Differential expression analysis of STOML2 between HCC and normal tissues was performed using the data from these cohorts. All analyses were conducted utilizing R version 4.0.3 (https://www.r-project.org/). The following R packages were used for data processing, analysis and visualization: 'limma' package (24) (version 3.46.0) and 'ggplot2' package (25) (version 3.3.5).

In silico protein interaction prediction. Potential interacting partners of STOML2 were predicted using the STRING database (version 11.0; https://string-db.org/). The search was performed using the full-length human STOML2 protein, with the minimum required interaction score set to the highest confidence (0.945).

Statistical analysis. Data from at least three independent experiments are presented as mean ± SD or median with interquartile range. Statistical significance was assessed using unpaired Student's t-test or Mann-Whitney U test for comparisons between groups. For paired comparisons such as between tumor and adjacent normal tissues from the same patients, the paired Student's t-test was used for normally distributed continuous data and the Wilcoxon signed-rank test was used for non-parametric or ordinal data (such as IHC scores). For comparisons among three or more groups, one- or two-way ANOVA was performed, followed by Tukey's post hoc test for multiple comparisons. $P<0.05$ was considered to indicate a statistically significant difference. GraphPad Prism 9.0 software (Dotmatics) was used for all statistical analyses.

Results

STOML2 expression is upregulated in HCC tissues. To explore the clinical relevance of STOML2 in HCC, patient survival was first analyzed using TCGA dataset via the GEPIA platform. The results indicated a significant association between high STOML2 expression and poor prognosis (Fig. 1A). Further analysis of two public datasets from the GEO confirmed that STOML2 expression was significantly upregulated in HCC tissues compared with that in paired normal liver tissues (Fig. 1C). In addition, STOML2 exhibited higher expression in the lung and adrenal metastatic lesions of patients with HCC compared with in healthy control patients (Fig. 1B). To further validate the expression of STOML2 in HCC tissues, immunohistochemical staining was performed on 72 paired HCC and adjacent non-tumor liver tissues. Notably, STOML2 protein levels were significantly higher in tumor tissues compared with those in control tissues (Fig. 1D and E). Additionally, the results of RT-qPCR and western blotting of samples from

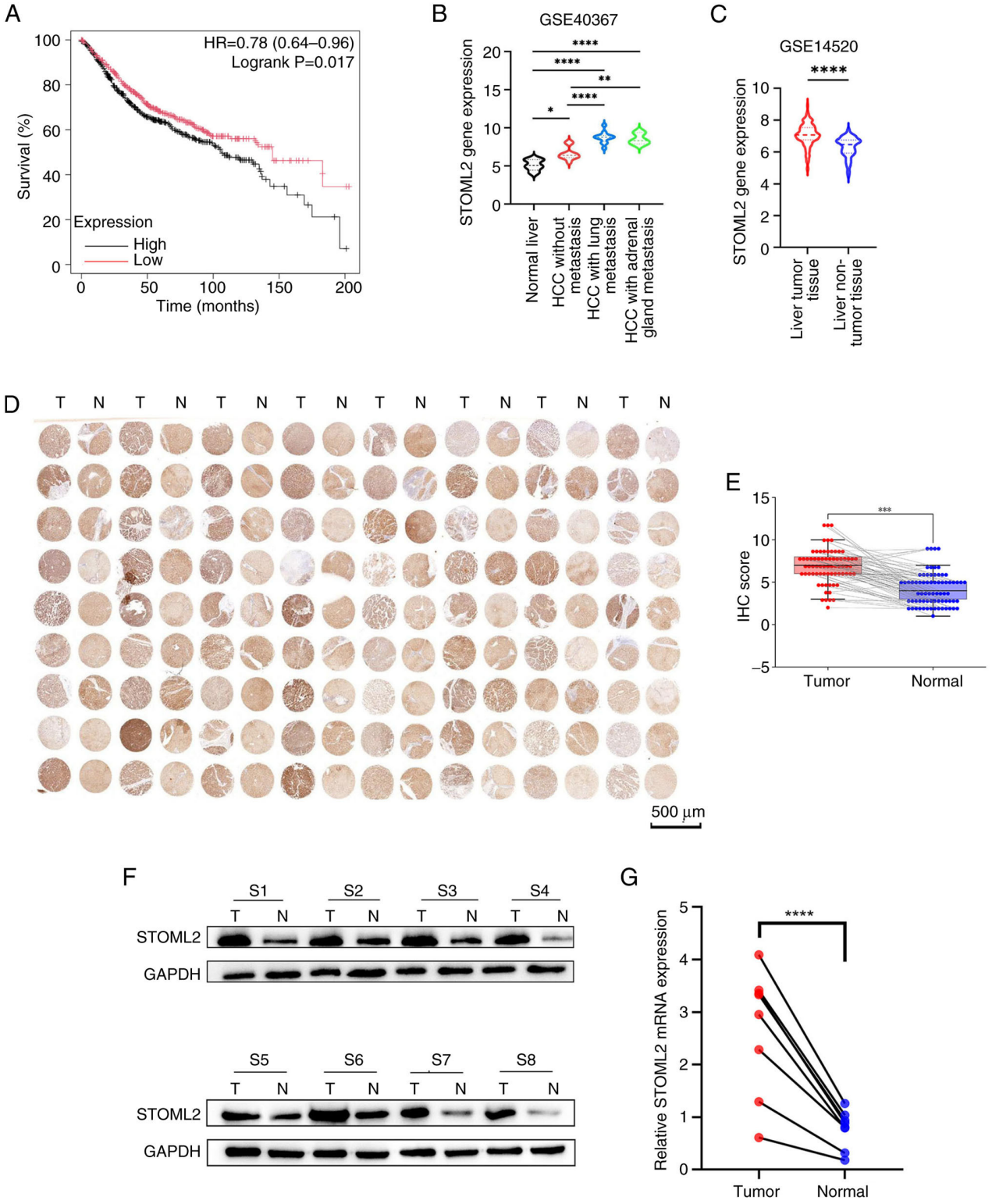

Figure 1. STOML2 expression is upregulated in HCC tissues. (A) Overall survival analysis using The Cancer Genome Atlas dataset showed that patients with HCC exhibiting high STOML2 expression had a significantly worse prognosis. P=0.017, log-rank test. (B and C) STOML2 expression levels across various cancer types determined using public datasets from the Gene Expression Omnibus. (B) GSE40367 dataset comparing normal liver tissue, non-metastatic HCC, HCC with lung metastasis and HCC with adrenal metastasis (*P<0.05, **P<0.01, ****P<0.0001, one-way ANOVA followed by Tukey's post hoc test, n=6, 10, 12 and 6, respectively). Data are presented as median with interquartile range. (C) GSE14520 dataset comparing HCC tissues and normal liver tissues (****P<0.0001, unpaired Student's t-test, n=65 and 50, respectively). Data are presented as median with interquartile range. (D) STOML2 protein expression in 72 paired HCC tissues (denoted as T) and adjacent normal tissues (denoted as N) was evaluated using IHC with tissue microarrays. (E) Semi-quantitative comparison of IHC staining (IHC score) for tumor tissues vs. adjacent normal tissues (n=72 pairs). Individual paired data points are shown as scatter plots, with lines connecting each tumor tissue to its matched adjacent normal tissue. The bars represent the median IHC score for each group, with error bars indicating the interquartile range. ***P<0.001, Wilcoxon signed-rank test. STOML2 expression was assessed in eight randomly selected paired HCC and normal tissues using (F) western blotting and (G) reverse transcription-quantitative polymerase chain reaction (n=8 pairs). (F) Representative images from three independent experiments are shown and (G) data were obtained from three independent experiments. ****P<0.0001, paired Student's t-test. Labels S1-S8 represent eight randomly selected paired HCC and adjacent normal tissue samples from individual patients. HCC, hepatocellular carcinoma; IHC, immunohistochemistry; STOML2, stomatin-like protein 2.

eight randomly selected patients with HCC further confirmed that the mRNA and protein levels of STOML2 were significantly higher in tumor tissues than in normal liver tissues (Fig. 1F and G). These findings indicated that STOML2 is consistently upregulated in HCC tissues and that it may serve a role in disease progression.

STOML2 promotes HCC cell proliferation, migration and invasion, induces autophagy and inhibits apoptosis. To investigate the role of STOML2 in HCC progression, the current study first examined its expression in liver cancer cell lines with varying metastatic potential, as well as in non-tumorigenic human hepatocyte cells, using western blotting and RT-qPCR (Fig. 2A). The results revealed that STOML2 was highly expressed in HCC cell lines compared with that in the non-tumorigenic human hepatocyte cell line THLE-2. Based on previous reports (26,27), the highly metastatic HCCLM3 cell line exhibits high endogenous STOML2 expression, making it suitable for knockdown experiments; conversely, the low metastatic Huh7 cell line displays relatively low STOML2 levels, rendering it appropriate for overexpression studies. Accordingly, the Huh7 cell line was infected with the STOML2-overexpression vector (Huh7-STOML2), whereas the HCCLM3 cell line was infected with shSTOML2 (HCCLM3-shSTOML2). Transduction efficiency was verified by western blotting and RT-qPCR (Fig. 2B). The CCK-8 (Fig. 2C), wound healing (Figs. 2D, S2D and S2E) and Transwell (Figs. 2G and S2A) assays showed that STOML2 overexpression promoted the proliferation, migration and invasion of Huh7 cells, whereas STOML2 knockdown reduced these malignant behaviors in HCCLM3 cells. The flow cytometric analysis revealed that STOML2 knockdown markedly inhibited cell cycle progression and decreased the proportion of S-phase HCCLM3 cells, whereas STOML2 overexpression had the opposite effect (Fig. 2E). In addition, flow cytometry showed that STOML2 overexpression inhibited late apoptosis in Huh7 cells, whereas STOML2 knockdown induced apoptosis in HCCLM3 cells (Fig. 2F). As available evidence links autophagy to enhanced cancer cell proliferation and invasion (28,29), the current study next examined the effect of STOML2 on autophagy-associated proteins (Fig. 2H). The results indicated that STOML2 overexpression promoted the proliferation and invasion of HCC cells and the level of autophagy-related proteins. By contrast, STOML2 knockdown suppressed the malignant phenotype and these autophagy-related markers.

STOML2 promotes HCC growth and progression in vivo. To investigate the oncogenic role of STOML2 *in vivo*, a subcutaneous tumor model was established in BALB/c nude mice. Tumor mass and growth curve analyses revealed that overexpression of STOML2 in Huh7 cells significantly promoted tumor growth (Fig. 3A-C). By contrast, knockdown of STOML2 in HCCLM3 cells markedly inhibited tumor growth. H&E staining showed notable changes in intercellular spacing within tumor tissues, but no marked differences in cellular morphology between the groups (Fig. 3E). The immunohistochemical analysis of Ki-67 showed that STOML2 knockdown significantly inhibited HCC proliferation *in vivo*, as indicated by lower Ki-67 expression (Fig. 3D). In summary, these *in vivo* findings provide direct evidence that STOML2 functions as a critical driver of HCC tumor growth.

STOML2 interacts with PHB and activates the RAF/MEK/ERK MAPK pathway. To elucidate the regulatory mechanism of STOML2 in HCC, the STRING database was used to predict potential STOML2-interacting proteins (Fig. S1B). PHB, a known chaperone of STOML2 (30), showed the highest binding score of 0.945 (Table SI). To further validate this interaction, co-IP was performed, which confirmed that STOML2 binds to PHB *in vitro* (Fig. 3F). IF staining of HCCLM3, HepG2 and Huh7 cells further revealed cytoplasmic co-localization of STOML2 and PHB (Fig. 3G). As PHB is known to serve an important role in the RAS-activated RAF/MEK/ERK signaling cascade, the current study assessed the phosphorylation status of key proteins in the MAPK pathway, p-RAF1, p-MEK1/2 and p-ERK1/2. The levels of these phosphorylated proteins were significantly elevated in STOML2-overexpressing Huh7 cells compared with in the control cells, and were significantly reduced in STOML2-knockdown HCCLM3 cells compared with in the knockdown control cells (Fig. 4A), indicating an opposing regulatory effect. Collectively, these results suggested that STOML2 interacts with PHB to activate the RAF/MEK/ERK MAPK signaling pathway, thereby promoting HCC progression.

PHB knockdown inhibits STOML2-induced migration, tumor growth, and autophagy and promotes apoptosis in HCC cells. To further investigate the role of PHB in STOML2-driven HCC progression, the current study first confirmed the knockdown efficiency of shPHB in parental Huh7 cells, which significantly reduced both PHB mRNA and protein levels compared with Scr (Fig. S1A). Subsequently, shPHB was introduced into Huh7 cells overexpressing STOML2. STOML2 overexpression upregulated PHB expression, and enhanced RAF, MEK and ERK phosphorylation; by contrast, PHB knockdown markedly reduced the phosphorylation of these MAPK pathway proteins (Fig. 4H). To evaluate the functional effect of PHB knockdown on Huh7-STOML2 cells, wound healing (Figs. 4B and S2F) and Transwell assays (Figs. 4D and S2B), and a cell cycle analysis (Fig. 4C) were performed. These assays demonstrated that PHB knockdown markedly attenuated STOML2-induced cell migratory and invasive capacity. Furthermore, flow cytometric analysis showed that the level of apoptosis was significantly increased in the PHB-knockdown group compared with that in the Scr group (Fig. 4F). *In vivo*, the subcutaneous implantation of Huh7-STOML2-shPHB cells into nude mice resulted in significantly slower tumor growth and smaller tumor volume than implantation of control cells (Fig. 4E, G and I). Western blotting further confirmed that PHB knockdown reduced autophagy-related protein levels in these cells compared with those in control cells (Fig. 4J). These *in vitro* and *in vivo* study findings indicated that PHB gene knockdown may significantly attenuate STOML2-induced migration and autophagy in HCC cells.

Sorafenib attenuates STOML2-induced migration and autophagy while promoting apoptosis in HCC cells. To elucidate the mechanism by which STOML2 regulates

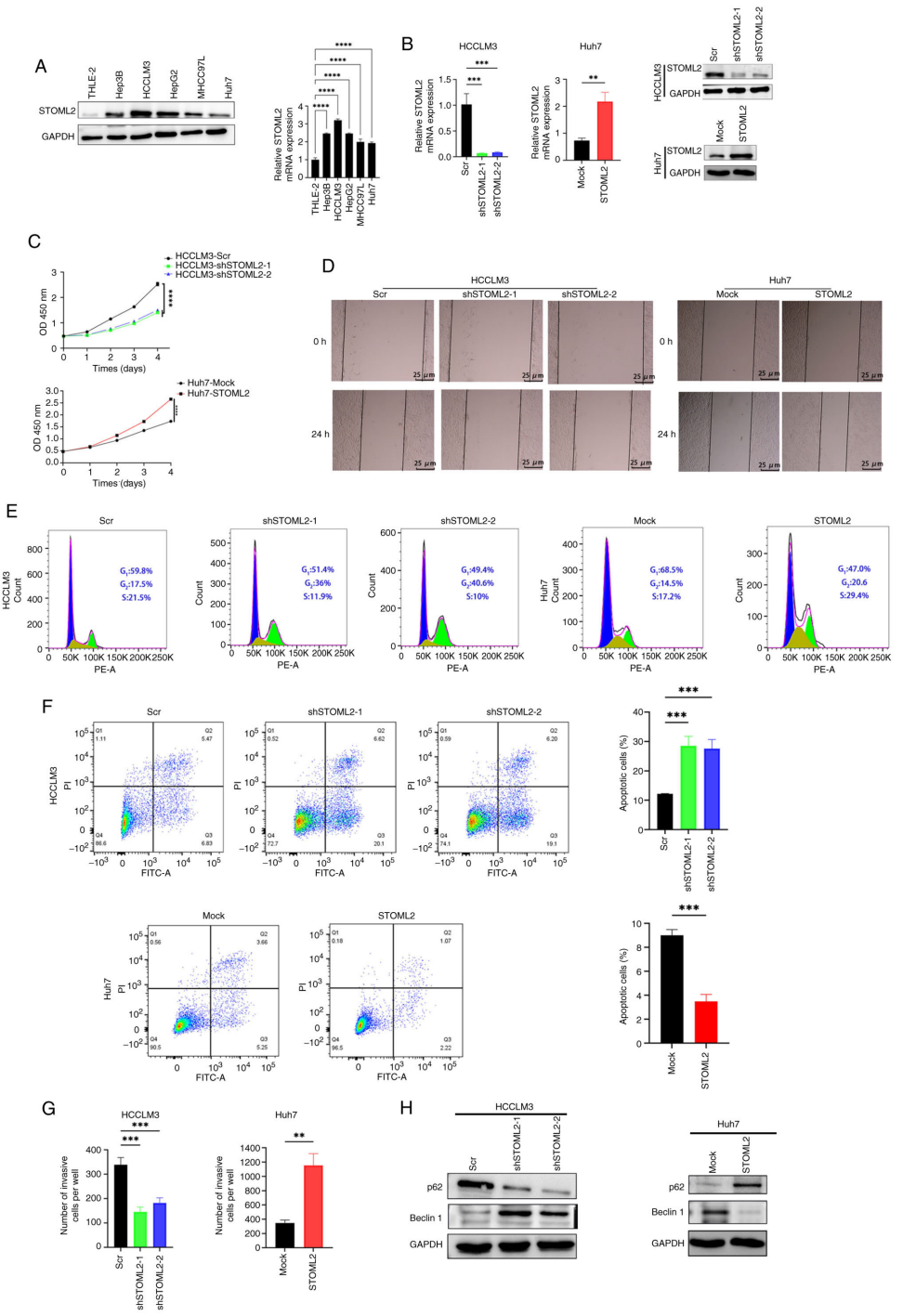

Figure 2. STOML2 promotes proliferation, migration, invasion and autophagy, and inhibits apoptosis in HCC cells. (A) STOML2 expression levels in five HCC cell lines and normal hepatocytes were determined using western blotting and RT-qPCR. Representative western blot images and quantitative RT-qPCR data (mean ± SD) from three independent experiments are shown (****P<0.0001, one-way ANOVA followed by Tukey's post-hoc tests). (B) Knockdown efficiency in HCCLM3 cells and overexpression efficiency in Huh7 cells were evaluated using western blotting and RT-qPCR. Representative western blot images and quantitative RT-qPCR data (mean ± SD) from three independent experiments are shown (***P<0.001, **P<0.01, comparisons between two groups were analyzed by unpaired Student's t-test, whereas comparisons among three groups were analyzed by one-way ANOVA followed by Tukey's post-hoc test). (C) Cell Counting Kit-8 assay showing the proliferation of STOML2-knockdown HCCLM3 cells, STOML2-overexpressing Huh7 cells and their respective controls. Data are presented as mean ± SD from three independent experiments (****P<0.0001, comparisons between two groups were analyzed by unpaired Student's t-test, whereas comparisons among three groups were analyzed by one-way ANOVA followed by Tukey's post-hoc test). (D) Wound healing assay assessing the migratory ability of STOML2-overexpressing or -knockdown HCC cells. Representative images from three independent experiments are shown. (E) Cell cycle distribution analysis of STOML2-knockdown HCCLM3 cells, STOML2-overexpressing Huh7 cells and their respective controls. Representative images from three independent experiments are shown. (F) Flow cytometric analysis of apoptosis rates of STOML2-overexpressing or -knockdown HCC cells along with their respective controls (***P<0.001, comparisons between two groups were analyzed by unpaired Student's t-test, whereas comparisons among three groups were analyzed by one-way ANOVA followed by Tukey's post-hoc test). Representative flow cytometry plots and quantitative data (mean ± SD) from three independent experiments are shown. (G) Transwell assay measuring the invasive capacity of HCC cells following STOML2 overexpression or knockdown (***P<0.001, **P<0.01, comparisons between two groups were analyzed by unpaired Student's t-test, whereas comparisons among three groups were analyzed by one-way ANOVA followed by Tukey's post-hoc test). Data are presented as mean ± SD. (H) Western blotting of autophagy markers p62 and Beclin1 in STOML2-overexpressing or -knockdown HCC cells. Representative western blot images from three independent experiments are shown. HCC, hepatocellular carcinoma; RT-qPCR, reverse transcription-quantitative polymerase chain reaction; Scr, scramble; sh, short hairpin; STOML2, stomatin-like protein 2.

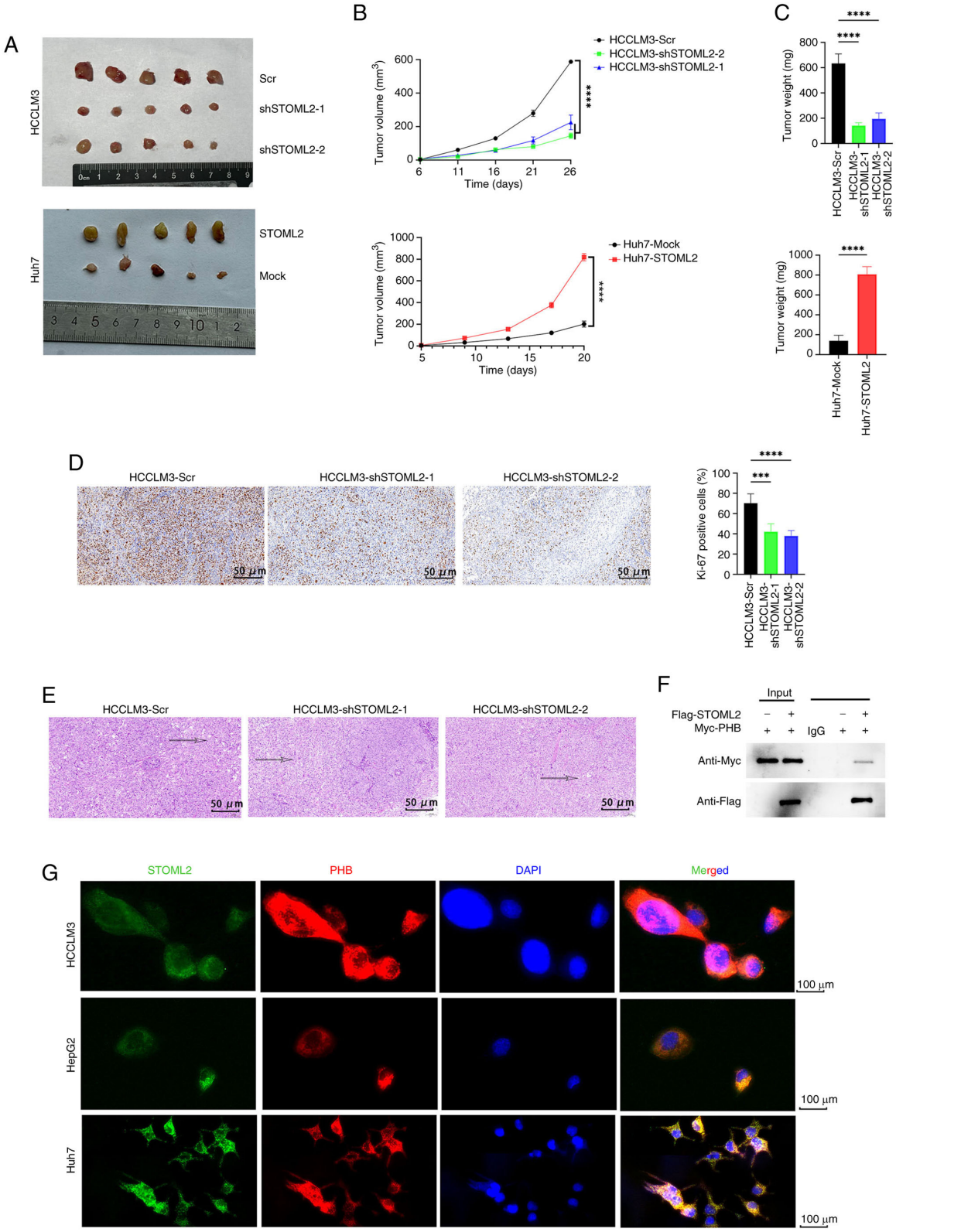

Figure 3. STOML2 promotes hepatocellular carcinoma growth and progression *in vivo*. (A-E) Subcutaneous implantation of STOML2-overexpressing Huh7 cells and STOML2-knockdown HCCLM3 cells along with their control cells in BALB/c nude mice. (A) Each mouse received $3x10^6$ cells as a subcutaneous injection at the dorsal region of their neck. Tumors were harvested 25 days post-injection. (B) Tumor growth curves obtained at the indicated time points (****P<0.0001, comparisons between two groups were analyzed by unpaired Student's t-test, whereas comparisons among three or more groups were analyzed by two-way ANOVA followed by Tukey's post hoc test). Data are presented as mean ± SD. (C) Final tumor mass measured upon removal (****P<0.0001, unpaired Student's t-test or one-way ANOVA and Tukey's post hoc test for multiple comparisons). Data are presented as mean ± SD. (D) Representative immunohistochemistry images showing a positive association between STOML2 and Ki-67 expression in tumor tissues. Quantitative data are presented as mean ± SD from multiple fields of view (****P<0.0001, ***P<0.001, one-way ANOVA followed by Tukey's post hoc test for multiple comparisons). (E) Representative hematoxylin and eosin staining of tumor sections. Images are representative of tumors from each group. (F) Co-immunoprecipitation assay demonstrating interaction between STOML2 and PHB *in vitro*. Representative western blot images from three independent experiments are shown. (G) Immunofluorescence staining showing colocalization of STOML2 (green), PHB (red) and DAPI (blue) in HCCLM3, HepG2 and Huh7 cells. Representative images from three independent experiments are shown. PHB, prohibitin; Scr, scramble; sh, short hairpin; STOML2, stomatin-like protein 2.

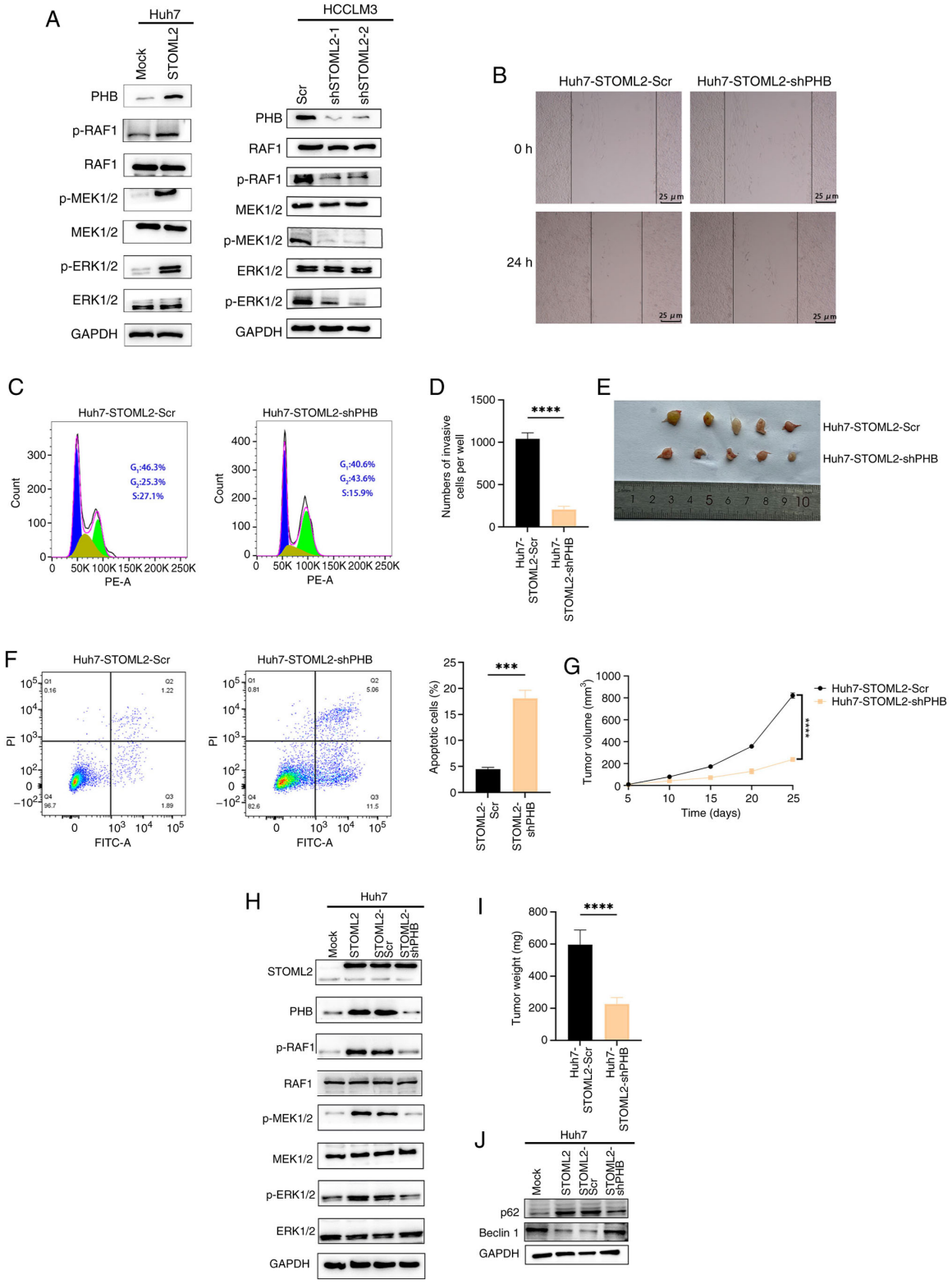

Figure 4. PHB knockdown inhibits STOML2-induced proliferation and invasion while promoting pro-apoptotic autophagy in HCC cells. (A) Western blot analysis of STOML2, PHB and key proteins of the MAPK signaling pathway in Huh7-STOML2, HCCLM3-shSTOML2 and their respective control cells. Representative western blot images from three independent experiments are shown. (B) Wound healing assay (scale bar, 25 μm), (C) cell cycle analysis and (D) Transwell assay (****P<0.0001, unpaired Student's t-test) demonstrating that PHB knockdown attenuated the cell cycle progression, migration and invasion of STOML2-overexpressing Huh7 cells. Representative images and quantitative analysis (mean ± SD) from three independent experiments are shown. (E) Huh7-STOML2-Scr control and Huh7-STOML2-shPHB cells were subcutaneously injected into BALB/c nude mice. Each mouse was injected with 3x10^6 cells in the dorsal region of their neck. (F) Flow cytometric analysis showing that PHB knockdown promoted apoptosis in STOML2-overexpressing Huh7 cells. Representative flow cytometry plots and quantitative data (mean ± SD) from three independent experiments are shown. (unpaired Student's t-test, ***P<0.001). (G) Tumor growth curves obtained at the indicated time points. Data are presented as mean ± SD (****P<0.0001, unpaired Student's t-test). (H) Western blotting of STOML2, PHB and MAPK signaling pathway proteins in Huh7-STOML2 cells with or without PHB knockdown. Representative western blot images from three independent experiments are shown. (I) Tumor mass measured at removal. ****P<0.0001, unpaired Student's t-test. Data are presented as mean ± SD. (J) Western blotting of p62 and Beclin1 in Huh7-STOML2 cells with or without PHB knockdown. Representative western blot images from three independent experiments are shown. p-, phosphorylated; PHB, prohibitin; Scr, scramble; sh, short hairpin; STOML2, stomatin-like protein 2.

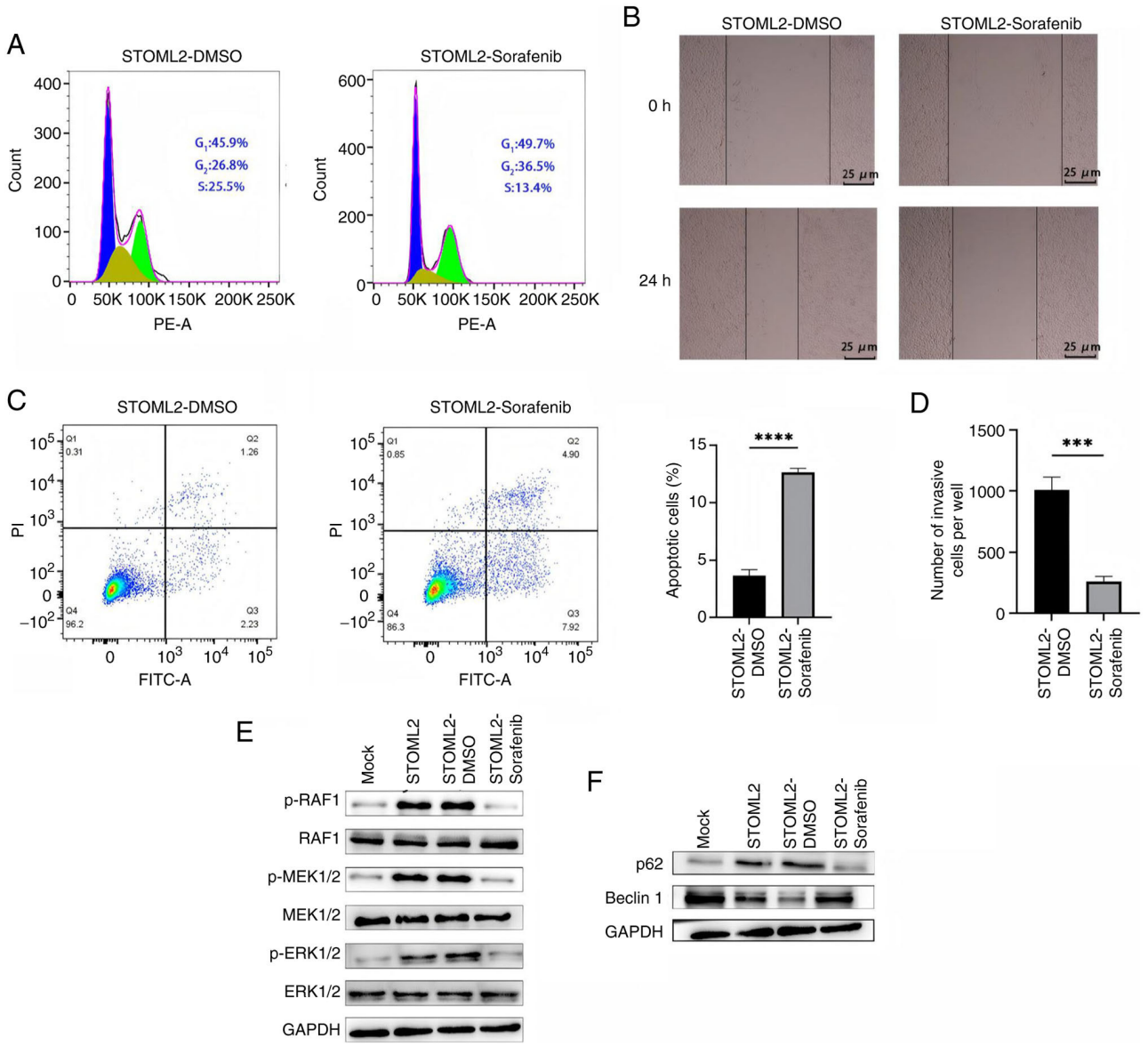

Figure 5. Sorafenib (an RAF1 inhibitor) significantly attenuated STOML2-induced cell cycle progression, migration and autophagy, while promoting apoptosis in HCC cells. (A) Cell cycle distribution analysis of Huh7-STOML2 and control cells following treatment with sorafenib (20 μM, 24 h) or DMSO. Representative images from three independent experiments are shown. (B) Wound healing assay showing the migratory capacity of Huh7-STOML2 cells treated with sorafenib or DMSO. Representative images from three independent experiments are shown. (C) Flow cytometric analysis of apoptosis in STOML2-overexpressing Huh7 and control cells after treatment with sorafenib or DMSO (unpaired Student's t-test, ****P<0.0001). Representative flow cytometry plots and quantitative data (mean ± SD) from three independent experiments are shown. (D) Transwell assay showing the invasive capacity of Huh7-STOML2 and control cells following sorafenib treatment or DMSO. Data are presented as mean ± SD (unpaired Student's t-test, ***P<0.001). Western blot analysis of (E) MAPK signaling pathway proteins, and (F) p62 and Beclin1 in Huh7-STOML2 cells after treatment with sorafenib or DMSO. Representative images from three independent experiments are shown. p-, phosphorylated; STOML2, stomatin-like protein 2.

the progression of HCC via the RAF/MEK/ERK MAPK signaling pathway, STOML2-overexpressing Huh7 cells were treated with the RAF1 inhibitor sorafenib. Sorafenib markedly inhibited the STOML2-induced phosphorylation of RAF, MEK and ERK, confirming inhibition of MAPK pathway activation (Fig. 5E). Sorafenib treatment also markedly attenuated the cell cycle progression, migration and invasion of Huh7 cells induced by STOML2 overexpression, as determined using cell cycle analyses (Fig. 5A), and wound healing (Figs. 5B and S2G) and Transwell (Figs. 5D and S2C) assays. Notably, although sorafenib further increased the levels of autophagy-related proteins (Fig. 5F), the flow cytometric analysis results showed a significant elevation in the level of apoptosis (Fig. 5C), suggesting that sorafenib may convert STOML2-driven 'protective autophagy' into pro-apoptotic signaling by blocking MAPK pathway activation. This observation is consistent with the results obtained for PHB-knockdown cells and reinforces the central role of the STOML2-PHB-MAPK axis in driving the malignant phenotype of HCC. Overall, these findings suggested that sorafenib may reverse the migration, invasion and autophagy-dependent survival advantage in HCC cells conferred by STOML2, while simultaneously inducing apoptosis by targeting and blocking STOML2-mediated activation of the MAPK pathway. These results provide mechanistic evidence supporting the use of sorafenib in patients with HCC and high STOML2 expression.

Discussion

The stomatin family of proteins is characterized by a conserved stomatin domain (30), which enables these proteins to carry out diverse cellular functions in various cell types, including membrane scaffolding and regulation of ion channel activity (31). As a member of this family, STOML2 (also known as SLP-2) is an inner mitochondrial membrane protein that has been implicated in protecting mitochondria from stress-induced hyperfusion (32). Increasing evidence has suggested that STOML2 expression is upregulated across multiple cancer types and is associated with poor prognosis (33,34). However, the mechanism of action of STOML2 in HCC cells remains unclear. The present study demonstrated that STOML2 was significantly upregulated in both HCC tissues and cell lines. Functional assays using STOML2 overexpression and knockdown models revealed STOML2 promoted HCC cell proliferation and invasion, underscoring its potential role as a pro-tumorigenic factor in HCC.

The stomatin proteins have been implicated in the regulation of transcription, energy metabolism, apoptosis and mitochondrial autophagy in tumor cells. Zheng *et al* (27) reported that STOML2 can promote HCC metastasis and drug resistance by directly binding to PTEN-induced kinase 1 (PINK1), stabilizing its half-life, and activating the PINK1-Parkin-dependent mitochondrial autophagy pathway. Under hypoxic conditions or following treatment with the antiangiogenic drug lenvatinib, HIF-1α-mediated upregulation of STOML2 triggers protective mitochondrial autophagy, thereby reducing drug efficacy. By contrast, inhibiting STOML2 activity or mitochondrial autophagy has been shown to significantly enhance the antitumor effects of lenvatinib (35). Notably, autophagy serves a crucial role in cancer progression (36). In pancreatic cancer, Qin *et al* (35) demonstrated that STOML2 may inhibit mitochondrial autophagy and enhance chemosensitivity by stabilizing presenilin-associated rhomboid-like proteins and accelerating PINK1 degradation. Although the mechanism contrasts with that of the STOML2-PINK1 axis in HCC, both studies underscore the central role of STOML2 in mitochondrial quality control. These tissue-specific differences may be influenced by variations in tumor microenvironment or genetic background, suggesting that the regulatory network of STOML2 should be investigated further. In the current study, STOML2 overexpression was revealed to inhibit apoptosis and induce the expression of autophagy-associated proteins in HCC cells. Emerging evidence has suggested that autophagy serves as a critical regulator of cell survival and death (37). This contrasts with the findings of Guo *et al* (38) in glioma, where the FoxM1-ubiquitin conjugating enzyme 2C axis was reported to promote tumor survival by suppressing autophagic cell death. These findings suggest that autophagy serves a dual role in cancer, with its net effect dependent on upstream regulatory pathways and stress conditions. Consequently, therapeutic targeting of STOML2 should be combined with the specific signaling landscape of the tumor to optimize its efficacy.

PHBs, mitochondrial proteins belonging to the same SPFH protein family as STOML2, participate in diverse cellular processes including proliferation, senescence, energy metabolism and assembly of the mitochondrial respiratory complexes (39). Notably, the protein levels of PHB-1 and PHB-2 have been shown to be markedly reduced in STOML2-depleted cells, suggesting that STOML2 may regulate PHB stability through direct or indirect interactions (40). Christie *et al* (41) demonstrated that STOML2 binds directly to PHB and that PHB-driven mitophagy partly explains how STOML2 regulates cell proliferation. In colorectal cancer, Ma *et al* (3) reported that STOML2 can promote tumor cell proliferation by activating the RAF/MEK/ERK pathway via binding to PHB, an effect reversed by PHB knockdown or RAF1 inhibition. The RAS proteins regulate key signaling pathways involved in both normal cellular growth and malignant transformation, mediating a broad spectrum of biological function (43,44). It has been well-documented that PHBs, which are ubiquitously expressed and evolutionarily conserved, are essential for RAS-mediated activation of the RAF/MEK/ERK pathway (44). In addition, PHBs are necessary for the membrane localization and activation of RAS to C-RAF *in vivo* (45). Consistent with these findings, the current study verified that STOML2 may directly interact with PHB in HCC using IF staining and co-IP assays in three HCC cell lines. Furthermore, it was demonstrated that PHB knockdown in STOML2-overexpressing HCC cells restored the effects of STOML2, promoting apoptosis, and suppressing both proliferation and the expression of autophagy-associated proteins. Together with previous evidence, the present study supports the hypothesis that STOML2 promotes cancer cell proliferation through the STOML2-PHB-MAPK signaling axis, which warrants further evaluation. Increasing evidence (46,47) has highlighted that the oncogenic role of STOML2 is characterized by synergistic activation of multiple pathways, establishing it as a critical tumor-promoting gene in HCC.

Sorafenib, a small-molecule multi-target kinase inhibitor, serves diverse roles in cancer therapy. It inhibits the MAPK pathway to suppress cell proliferation, blocks receptor tyrosine kinases such as platelet-derived growth factor receptor and vascular endothelial growth factor receptor to reduce tumor angiogenesis, and promotes apoptosis (48). Sorafenib is currently approved by the United States Food and Drug Administration for the treatment of renal cell carcinoma, advanced HCC and differentiated thyroid cancer (49). In the present study, sorafenib attenuated STOML2-induced migration and cell cycle progression in HCC, and enhanced apoptosis while inhibiting MAPK signaling. However, the inhibitory effects of sorafenib are broad and not specific to the MAPK pathway; therefore, its use in HCC treatment needs to be further evaluated. Despite the success of targeted therapies for cancer, the widespread emergence of drug resistance remains a major clinical challenge (50).

Notably, previous studies (51,52) on mitochondria-related genes further support the pivotal role of STOML2 in HCC. For example, the downregulation of ferredoxin 1 (FDX1), a mitochondrial iron-sulfur cluster synthase, has been shown to activate mitochondrial autophagy and promote HCC progression via reactive oxygen species accumulation (53). Similar to that of STOML2, dysregulation of FDX1 leads to metabolic reprogramming and enhances tumor cell adaptability. This suggests that mitochondrial homeostatic regulatory genes such as STOML2 and FDX1 may form a synergistic network contributing to HCC development. Future studies should investigate potential interactions between STOML2 and genes

such as FDX1 to elucidate more complex mitochondrial regulatory mechanisms in liver cancer.

In summary, the present study systematically elucidated the mechanism by which STOML2 regulates autophagy to promote HCC progression via the PHB-MAPK axis. Combined with the existing literature, the current findings further highlight the multifaceted role of STOML2 as a mitochondrial hub protein. Future studies are recommended to expand upon this work in several important directions. First, it is necessary to investigate whether STOML2 synergizes with other mitochondrial proteins, such as FDX1, in driving HCC metabolic reprogramming, particularly at the intersection between mitochondrial energy metabolism and oxidative stress. Second, the mechanisms regulating STOML2 expression remain unclear. Potential regulatory factors such as the microRNA-200 family or epigenetic modifications (such as DNA methylation) warrant exploration and may offer new strategies for targeted intervention. Third, combination therapies targeting the STOML2-PHB-MAPK axis, such as co-administering sorafenib with autophagy inhibitors, could exhibit enhanced efficacy by synergistically blocking pro-oncogenic signaling; these should be evaluated in preclinical models. Finally, for STOML2 to transition from a molecular target to a clinically applicable biomarker, systematic validation of its utility in patient stratification, prognosis prediction and therapeutic response monitoring is needed. Advancing these areas of research will provide a more comprehensive understanding of the pathological importance of STOML2 and may offer innovative strategies to improve the prognosis of patients with HCC.

The present study demonstrated that STOML2 was significantly upregulated in HCC, and indicated that it may promote cancer cell proliferation and tumor growth by interacting with PHB and activating the MAPK signaling pathway to mediate autophagy. These findings suggest that STOML2 may serve as a novel biomarker and potential therapeutic target in HCC.

Acknowledgements

Not applicable.

Funding

The present study was supported by the Health Commission of Hebei Province (grant no. 3101030211003).

Availability of data and materials

The data generated in the present study may be requested from the corresponding author.

Authors' contributions

HH and HZ were involved in the conception and design of the study. HH and SH performed the experiments and collected the data. HH, YX and JC were responsible for data analysis, interpretation and validation, and confirm the authenticity of all the raw data. HH wrote the original draft. HZ, SH, YX and JC reviewed and edited the manuscript. All authors read and approved the final manuscript.

Ethics approval and consent to participate

The study involving human participants was approved by the Ethics Committee of the North China University of Science and Technology Affiliated Hospital (approval no. 20250403024). All procedures were conducted in accordance with the ethical standards of the responsible committees on human experimentation at our institution and with the national bioethical regulations of the People's Republic of China. Furthermore, the study was performed in compliance with the tenets of the 1964 Declaration of Helsinki. All patients provided written informed consent. The animal experiments performed in the present study were approved by the Animal Ethics Committee of North China University of Science and Technology, (approval no. 2025SY3011).

Patient consent for publication

Not applicable.

Competing interests

The authors declare that they have no competing interests.

References

1. Sung H, Ferlay J, Siegel RL, Laversanne M, Soerjomataram I, Jemal A and Bray F: Global cancer statistics 2020: GLOBOCAN estimates of incidence and mortality worldwide for 36 cancers in 185 countries. CA Cancer J Clin 71: 209-249, 2021.
2. De Toni EN, Schlesinger-Raab A, Fuchs M, Schepp W, Ehmer U, Geisler F, Ricke J, Paprottka P, Friess H, Werner J, *et al*: Age independent survival benefit for patients with hepatocellular carcinoma (HCC) without metastases at diagnosis: A population-based study. Gut 69: 168-176, 2020.
3. Ma W, Chen Y, Xiong W, Li W, Xu Z, Wang Y, Wei Z, Mou T, Wu Z, Cheng M, *et al*: STOML2 interacts with PHB through activating MAPK signaling pathway to promote colorectal cancer proliferation. J Exp Clin Cancer Res 40: 359, 2021.
4. Keum N and Giovannucci E: Global burden of colorectal cancer: Emerging trends, risk factors and prevention strategies. Nat Rev Gastroenterol Hepatol 16: 713-732, 2019.
5. Pinter M, Scheiner B and Pinato DJ: Immune checkpoint inhibitors in hepatocellular carcinoma: Emerging challenges in clinical practice. Lancet Gastroenterol Hepatol 8: 760-770, 2023.
6. Owczarek CM, Treutlein HR, Portbury KJ, Gulluyan LM, Kola I and Hertzog PJ: A novel member of the STOMATIN/EPB72/mec-2 family, stomatin-like 2 (STOML2), is ubiquitously expressed and localizes to HSA chromosome 9p13.1. Cytogenet Cell Genet 92: 196-203, 2001.
7. Wang Y and Morrow JS: Identification and characterization of human SLP-2, a novel homologue of stomatin (band 7.2b) present in erythrocytes and other tissues. J Biol Chem 275: 8062-8071, 2000.
8. Mitsopoulos P, Chang Y, Wai T, König T, Dunn SD, Langer T and Madrenas J: Stomatin-like protein 2 is required for in vivo mitochondrial respiratory chain supercomplex formation and optimal cell function. Mol Cell Biol 35: 1838-1847, 2015.
9. Mitsopoulos P, Lapohos O, Weraarpachai W, Antonicka H, Chang Y and Madrenas J: Stomatin-like protein 2 deficiency results in impaired mitochondrial translation. PLoS One 12: e0179967, 2017.
10. Guo X, Guo H and Guo H: Clinical significance of SLP-2 in epithelial ovarian cancer and its regulatory effect on the Notch signaling pathway. Eur Rev Med Pharmacol Sci 24: 1666-1671, 2020.
11. Wang WX, Lin QF, Shen D, Liu SP, Mao WD, Ma G and Qi WD: Clinicopathological significance of SLP-2 overexpression in human gallbladder cancer. Tumour Biol 35: 419-423, 2014.
12. Zhang J, Song X, Li C and Tian Y: Expression and clinical significance of SLP-2 in ovarian tumors. Oncol Lett 17: 4626-4632, 2019.

13. Liu D, Zhang L, Shen Z, Tan F, Hu Y, Yu J and Li G: Increased levels of SLP-2 correlate with poor prognosis in gastric cancer. Gastric Cancer 16: 498-504, 2013.
14. Attia AS, Hussein S, Sameh H, Khalil A, Waley AB, Matar I and Sameh R: Diagnostic and prognostic utility of TROP-2, SLP-2, and CXCL12 expression in papillary thyroid carcinoma. Cancer Biomark 39: 211-221, 2024.
15. Zhou C, Li Y, Wang G, Niu W, Zhang J, Wang G, Zhao Q and Fan L: Enhanced SLP-2 promotes invasion and metastasis by regulating Wnt/β-catenin signal pathway in colorectal cancer and predicts poor prognosis. Pathol Res Pract 215: 57-67, 2019.
16. Yin R, Tao Y, Han J, Zhang J, Yu K, Zheng Y, Li X and Huang C: STOML2 inhibits sorafenib-induced ferroptosis in hepatocellular carcinoma via p-AKT signaling pathway. Am J Cancer Res 15: 1614-1628, 2025.
17. Qu H, Jiang W, Wang Y and Chen P: STOML2 as a novel prognostic biomarker modulates cell proliferation, motility and chemo-sensitivity via IL6-Stat3 pathway in head and neck squamous cell carcinoma. Am J Transl Res 11: 683-695, 2019.
18. Shao YY, Shau WY, Chan SY, Lu LC, Hsu CH and Cheng AL: Treatment efficacy differences of sorafenib for advanced hepatocellular carcinoma: A meta-analysis of randomized clinical trials. Oncology 88: 345-352, 2015.
19. Kitano K, Murayama T, Sakamoto M, Nagayama K, Ueno K, Murakawa T and Nakajima J: Outcome and survival analysis of pulmonary metastasectomy for hepatocellular carcinoma. Eur J Cardiothorac Surg 41: 376-382, 2012.
20. Livak KJ and Schmittgen TD: Analysis of relative gene expression data using real-time quantitative PCR and the 2(-delta delta c(t)) method. Methods 25: 402-408, 2001.
21. Shi Y, Wang Y, Zhang W, Niu K, Mao X, Feng K and Zhang Y: N6-methyladenosine with immune infiltration and PD-L1 in hepatocellular carcinoma: Novel perspective to personalized diagnosis and treatment. Front Endocrinol (Lausanne) 14: 1153802, 2023.
22. Roessler S, Lin G, Forgues M, Budhu A, Hoover S, Simpson RM, Wu X, He P, Qin L, Tang Z, *et al*: Integrative genomic and transcriptomic characterization of matched primary and metastatic liver and colorectal carcinoma. Int J Biol Sci 11: 88-98, 2015.
23. Ji F, Zhang J, Mao L, Tan Y, Ye M, He X, Zhao Y, Liu J, Zhang Y, Zhang N, *et al*: Liver-specific gene PGRMC1 blocks c-Myc-induced hepatocarcinogenesis through ER stress-independent PERK activation. Nat Commun 16: 50, 2025.
24. Ritchie ME, Phipson B, Wu D, Hu Y, Law CW, Shi W and Smyth GK: Limma powers differential expression analyses for RNA-sequencing and microarray studies. Nucleic Acids Res 43: e47, 2015.
25. Cao T, Li Q, Huang Y and Li A: plotnineSeqSuite: A Python package for visualizing sequence data using ggplot2 style. BMC Genomics 24: 585, 2023.
26. Li X, Zheng Y, Yu K, Hou S, Cui H, Yin R, Zhou Y, Sun Q, Zhang J and Huang C: Stomatin-like protein 2 promotes cell proliferation and survival under 5-fluorouracil stress in hepatocellular carcinoma. Mol Biol Rep 51: 228, 2024.
27. Zheng Y, Huang C, Lu L, Yu K, Zhao J, Chen M, Liu L, Sun Q, Lin Z, Zheng J, *et al*: STOML2 potentiates metastasis of hepatocellular carcinoma by promoting PINK1-mediated mitophagy and regulates sensitivity to lenvatinib. J Hematol Oncol 14: 16, 2021.
28. Liu P, Li L, Wang W, He C and Xu C: MST4 promotes proliferation, invasion, and metastasis of gastric cancer by enhancing autophagy. Heliyon 9: e16735, 2023.
29. He R, Liu Y, Fu W, He X, Liu S, Xiao D and Tao Y: Mechanisms and cross-talk of regulated cell death and their epigenetic modifications in tumor progression. Mol Cancer 23: 267, 2024.
30. Genin EC, Bannwarth S, Ropert B, Lespinasse F, Mauri-Crouzet A, Augé G, Fragaki K, Cochaud C, Donnarumma E, Lacas-Gervais S, *et al*: CHCHD10 and SLP2 control the stability of the PHB complex: A key factor for motor neuron viability. Brain 145: 3415-3430, 2022.
31. Lapatsina L, Brand J, Poole K, Daumke O and Lewin GR: Stomatin-domain proteins. Eur J Cell Biol 91: 240-245, 2012.
32. Tondera D, Grandemange S, Jourdain A, Karbowski M, Mattenberger Y, Herzig S, Da Cruz S, Clerc P, Raschke I, Merkwirth C, *et al*: SLP-2 is required for stress-induced mitochondrial hyperfusion. EMBO J 28: 1589-1600, 2009.
33. Cui Z, Zhang L, Hua Z, Cao W, Feng W and Liu Z: Stomatin-like protein 2 is overexpressed and related to cell growth in human endometrial adenocarcinoma. Oncol Rep 17: 829-833, 2007.
34. Wang Y, Cao W, Yu Z and Liu Z: Downregulation of a mitochondria associated protein SLP-2 inhibits tumor cell motility, proliferation and enhances cell sensitivity to chemotherapeutic reagents. Cancer Biol Ther 8: 1651-1658, 2009.
35. Qin C, Wang Y, Zhao B, Li Z, Li T, Yang X, Zhao Y and Wang W: STOML2 restricts mitophagy and increases chemosensitivity in pancreatic cancer through stabilizing PARL-induced PINK1 degradation. Cell Death Dis 14: 191, 2023.
36. Niu X, You Q, Hou K, Tian Y, Wei P, Zhu Y, Gao B, Ashrafizadeh M, Aref AR, Kalbasi A, *et al*: Autophagy in cancer development, immune evasion, and drug resistance. Drug Resist Updat 78: 101170, 2025.
37. Klionsky DJ, Petroni G, Amaravadi RK, Baehrecke EH, Ballabio A, Boya P, Bravo-San Pedro JM, Cadwell K, Cecconi F, Choi AMK, *et al*: Autophagy in major human diseases. EMBO J 40: e108863, 2021.
38. Guo L, Ding Z, Huang N, Huang Z, Zhang N and Xia Z: Forkhead Box M1 positively regulates UBE2C and protects glioma cells from autophagic death. Cell Cycle 16: 1705-1718, 2017.
39. Mcclung JK, Jupe ER, Liu XT and Dell'Orco RT: Prohibitin: Potential role in senescence, development, and tumor suppression. Exp Gerontol 30: 99-124, 1995.
40. Da Cruz S, Parone PA, Gonzalo P, Bienvenut WV, Tondera D, Jourdain A, Quadroni M and Martinou JC: SLP-2 interacts with prohibitins in the mitochondrial inner membrane and contributes to their stability. Biochim Biophys Acta 1783: 904-911, 2008.
41. Christie DA, Lemke CD, Elias IM, Chau LA, Kirchhof MG, Li B, Ball EH, Dunn SD, Hatch GM and Madrenas J: Stomatin-like protein 2 binds cardiolipin and regulates mitochondrial biogenesis and function. Mol Cell Biol 31: 3845-3856, 2011.
42. Downward J: Targeting RAS signalling pathways in cancer therapy. Nat Rev Cancer 3: 11-22, 2003.
43. Wellbrock C, Karasarides M and Marais R: The RAF proteins take centre stage. Nat Rev Mol Cell Biol 5: 875-885, 2004.
44. Xu L, Meng L, Xiang W, Wang X, Yang J, Shu C, Zhao XH, Rong Z and Ye Y: Prohibitin 2 confers NADPH oxidase 1-mediated cytosolic oxidative signaling to promote gastric cancer progression by ERK activation. Free Radic Biol Med 224: 130-143, 2024.
45. Sharma A and Qadri A: Vi polysaccharide of salmonella typhi targets the prohibitin family of molecules in intestinal epithelial cells and suppresses early inflammatory responses. Proc Natl Acad Sci USA 101: 17492-17497, 2004.
46. Ma W, Xu Z, Wang Y, Li W, Wei Z, Chen T, Mou T, Cheng M, Luo J, Luo T, *et al*: A positive feedback loop of SLP2 activates MAPK signaling pathway to promote gastric cancer progression. Theranostics 8: 5744-5757, 2018.
47. Wai T, Saita S, Nolte H, Müller S, König T, Richter-Dennerlein R, Sprenger HG, Madrenas J, Mühlmeister M, Brandt U, *et al*: The membrane scaffold SLP2 anchors a proteolytic hub in mitochondria containing PARL and the i-AAA protease YME1L. EMBO Rep 17: 1844-1856, 2016.
48. Lierman E, Lahortiga I, Van Miegroet H, Mentens N, Marynen P and Cools J: The ability of sorafenib to inhibit oncogenic PDGFRbeta and FLT3 mutants and overcome resistance to other small molecule inhibitors. Haematologica 92: 27-34, 2007.
49. Abdelgalil AA, Alkahtani HM and Al-Jenoobi FI: Sorafenib. Profiles Drug Subst Excip Relat Methodol 44: 239-266, 2019.
50. Fischer PM: Approved and experimental small-molecule oncology kinase inhibitor drugs: A mid-2016 overview. Med Res Rev 37: 314-367, 2017.
51. Tsvetkov P, Detappe A, Cai K, Keys HR, Brune Z, Ying W, Thiru P, Reidy M, Kugener G, Rossen J, *et al*: Mitochondrial metabolism promotes adaptation to proteotoxic stress. Nat Chem Biol 15: 681-689, 2019.
52. Lin X, Zheng J, Li Y, Liu L, Liu Q, Lin J and Sun Y: Mitochondria-related genes as prognostic signature of endometrial cancer and the effect of MACC1 on tumor cells. PLoS One 20: e0323002, 2025.
53. Sun B, Ding P, Song Y, Zhou J, Chen X, Peng C and Liu S: FDX1 downregulation activates mitophagy and the PI3K/AKT signaling pathway to promote hepatocellular carcinoma progression by inducing ROS production. Redox Biol 75: 103302, 2024.